Journal of Visualization, Vol. 6, No. 4 (2003) 381-393

Automotive Testing Using Pressure-Sensitive Paint

Mébarki, Y.*[1], Cooper, K. R.*[1] and Reichert, T. M.*[2]

*1 Institute for Aerospace Research, National Research Council
1200 Montreal Road, Ottawa, K1A0R6, Canada.
Tel: (613) 998 8994, Fax: (613) 998 1281
E-mail: youssef.mebarki@nrc.ca
*2 Student, Engineering Science Program, University of Toronto, Canada.

Received 31 October 2002
Revised 25 April 2003

Abstract : Measurements of the surface pressure on a simplified automobile model have been performed using pressure-sensitive paint (PSP). The program was undertaken to investigate the use of commercial and in-house PSP at low speed (between 11 m/s and 92 m/s) and to find techniques to improve the measurement accuracy. A comparison of *a priori* and *in situ* calibration methods was also conducted. A linear *in situ* calibration or *a priori* methods combined with one tap pressure, correcting for bias errors, were found to provide the best accuracy.

Keywords : Visualization, PSP, Automotive testing, Pressure measurements.

1. Introduction

The pressure-sensitive paint (PSP) technique is an optical method widely used in wind tunnel testing to obtain surface pressure measurements. This well-documented technique (Liu et al., 1992; Crites, 1993; Bell et al., 2001; Yves Le Sant et al., 2001), is based on the luminescence quenching of fluorescent molecules by oxygen. In order to achieve greater accuracy in wind tunnel testing, recent efforts have focused on the PSP formulation improvement (Benne et al. 2002) and on the combination of PSP with a temperature sensitive component to correct for temperature variations (Mitsuo et al., 2002; Khalil et al., 2002). Although very promising, these binary paint formulations can complicate wind tunnel tests compared to single-sensor formulations. Means of switching the emission range are required: two (or more) detectors are needed when a filter wheel or a prism image splitter (Kulesh et al., 2001) is not available.

The goal of this study is to assess the accuracy of single component PSP formulations using a simplified car model in the IAR 2 m x 3 m low-speed wind tunnel. The choice of the low-speed regime for this study is justified by the fact that greater resolution and accuracy is required when the pressure variation on the model is small, as is the case in low-speed tests. This paper presents and compares different data reduction schemes applied to commercial and in-house PSP formulations evaluated at various wind speeds ($11\ m/s < V < 92\ m/s$) and model yaw angles ($-25° < \Psi < 25°$). In addition, to further support the PSP results, oil flow visualizations were done at yaw angles of 0° and ±20°.

2. Material

2.1 Facility

The IAR 2 m x 3 m, low-speed wind tunnel is a closed-return, continuous-flow, atmospheric facility equipped with a 2.7m-wide, 1.7m-high, filleted test section and ground board used for automotive testing. The maximum tunnel speed with the ground board installed is 110 m/s.

2.2 Model

For these tests a simplified automobile model was used. This model has the general form of a passenger car, but without wheels, and can be fitted with four interchangeable rear-end shapes that provide the base flow fields of the most common automotive forms – hatch-back, wagon-back, notch-back and fast-back. For the present PSP evaluation, a notch-back model of 1:7.8-scale was selected. This model was manufactured at IAR and was made of mahogany, with some aluminium parts. The model is l = 533.4 mm long, 203.2 mm wide and 101.6 mm high. A photograph of the painted model in the test section is shown in Fig. 1.

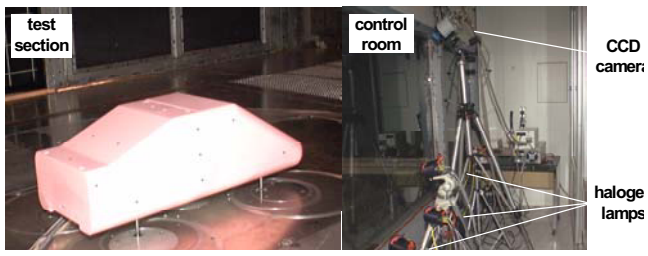

Fig. 1. Painted model in the 2 m x 3 m wind tunnel (left) with illumination and acquisition system looking through the side window (right photo). Targets (black dots) on the model are used for image registration.

The model was instrumented with a total of 81 pressure taps distributed over the model top surface (64) and bottom surface (17). Up to 34 taps were used to assess the PSP accuracy.

These are shown in Fig. 2 and are grouped in seven different stations. Station 1, located on the model centerline (z=0), covers almost the entire model length (from x/l=0 to 1). On this station, the two pressure orifices on the front (Tap A) and rear (Tap B) windshield headers were added after the first set of tests to capture the suction peaks due to the high flow curvature at these locations. The PSP measurements, obtained in the first instance, were used to determine the exact locations of the minimum pressures on the model and to direct this additional tap implementation.

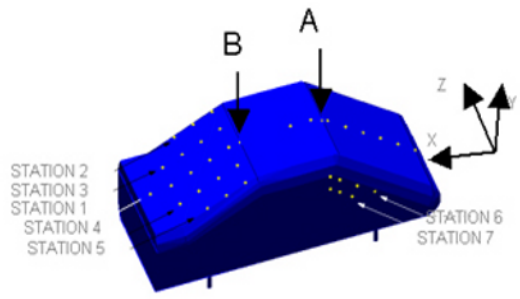

Fig. 2. Pressure orifices used for comparison with PSP.

2.3 Measurement Techniques

Discrete pressures on the model were measured using a HyScan 2000™ scanning system equipped with a 2.5-Pa, 64-port, ZOC-33 scanner module installed in the model. Discrete temperatures were obtained from Omegafilm RTDs(model F3101) that were calibrated against a Hart Scientific (model 9107) calibrator to within ±0.03°C. Surface temperature measurements were also made using an Agema Thermovision 900 camera looking through an orifice in the ceiling of the test section. The infrared system, using a single Stirling-cooled detector, sensitive in the 8 - 12 μm region, provided an image of 272 × 136 pixels. The PSP emissivity was determined from laboratory calibration using a paint sample placed on a thermoelectrically controlled plate. The paint emissivity was found to be fairly uniform from 10°C to 34°C and ranged from 0.695 to 0.746, depending on the PSP coating.

During the PSP tests, the infrared measurements were accurate to within 1°C when compared to the discrete temperature sensors (RTD) placed on the model. Surface temperature data from these sensors was systematically used to perform a linear calibration of the infrared measurements. The accuracy of the infrared measurement was 0.14°C RMS averaged over a total of 97 wind-on and wind-off images.

2.4 PSP System

The model was first primed with a Tristar Starpoxy fluid resistant white epoxy primer (DHMS C4.01 Ty3). Between the PSP evaluations, the painted car model was cleaned using acetone without damaging the primer. Two commercial formulations, Unifib and Unicoat both using the Platinum tetra(trisfluorophenyl)porphyrin (PtTFPP) as the luminophore, were supplied by Innovative Scientific Solutions Inc. (ISSI). Two in-house formulations, based on pyrene, were also evaluated. The first pyrene formulation, referred to as NRM2, consists of 7 mM of pyrene (Sigma Aldrich) per liter of resin RTV118 (General Electric). The second, referred to as NPM2, is composed of 70 mM of pyrene in poly(TMSP) (Mérienne, 2001; Asai et al., 2002) provided by Gelest Inc. Table 1 compares the slopes of the pressure and temperature sensitivities of the different paints under investigation. The good performance of the pyrene-based paints, i.e. high pressure sensitivity and low temperature sensitivity, is counterbalanced by the pyrene sublimation from the binder (Mérienne and Soumagne-Schweyckart, 2002), which induces significant ageing, or loss of performance with time (e.g. intensity reduction, sensitivity changes).

Table 1. Characteristics of the PSP formulations evaluated.

PSP	Binder	Luminophore	SP (% per bar) @ 20°C	ST (% per deg.) @ 1 bar
Unifib	FIB	PtTFPP	79	-0.42
Unicoat	N/D	PtTFPP	61	-1.60
NRM2	RTV118	Pyrene	92	-0.20
NPM2	PTMSP	Pyrene	81	0.30

Excitation in the visible range was provided by air-cooled green Halogen lamps (flood Iwasaki JY1562 50 W) filtered with a color filter (Kopp 4-96). When needed, ultraviolet excitation was provided by a filtered 200 W Hg-Xe Hamamatsu UV-SPOT (model L8333) light source using an optical fiber. The PSP emission was recorded with a 12-bit, 1024 × 1024 pixel Photometrics camera, mostly used in 2 x 2 pixel binning mode, in which every 4-pixel square is combined to form a new single pixel, thus reducing the actual spatial resolution to 512 x 512 pixels. The camera was equipped with two Andover 650FS40 and 650FS80 filters in parallel, for the porphyrin-based paints, and with one blue-green 500FS80 Andover filter for the pyrene paints.

3. Test Planning

The test program was conducted in three phases. The first test phase was limited to the study of the commercial Unifib and Unicoat paint formulations using visible (green) light excitation. During the second phase of testing, an ultraviolet light source was used to excite the pyrene-based paints (NRM2 and NPM2) as well as the Unifib paint. The third phase was a repeat of the first phase (Unifib and Unicoat with green excitation), but with the tap addition on the front and rear windshield headers.

During the last phase of the test, the pressure scanners in the model were operated without heating, whereas in the early phases the ZOC-module in the model was heated to 30ºC to stabilize its operating temperature. RTD temperature measurements were made using either one or three

RTD's on the model roof near the centerline at $x/l = 0.16$, $x/l = 0.48$ and $x/l = 0.80$, l being the model length. The infrared camera was only used during the last phase. As the Unicoat formulation withstands manipulation and thorough cleaning, oil-flow visualizations were performed with this paint at the end of evaluation (phases 1 and 3). The wind speed varied from $V = 11$ m/s to 92 m/s with yaw angles ranging from -25° to 25°. Table 2 summarizes the various configurations. Several yaw angles were acquired per run, except in the first phase and with the pyrene formulations in the second phase, for which only one angle per run was acquired so as to reduce the time and the possible photodegradation between the wind-off and wind-on measurements.

Table 2. Summary of the test conditions.

Phase	PSP	Excitation	Speeds (m/s)	Yaw range (deg.)	RTD on model	Infrared camera	Oil Flow Vis
1	Unifib	Green	41, 62, 77, 92	-20 to 20	1	-	-
	Unicoat	Green	41, 62, 77, 92	-20 to 20	1	-	Yes
2	NPM2	UV	41, 62, 77, 92	-20 to 20	1	-	-
	NRM2	UV	41, 92	-20 to 20	1	-	-
	Unifib	UV	41, 61, 92	-25 to 25	0	-	-
3	Unifib	Green	11, 27, 41, 92	-25 to 25	3	Yes	-
	Unicoat	Green	27, 41, 92	-20 to 20	3	Yes	Yes

4. PSP Data Reduction

The main steps in the PSP data reduction used in this study have been described extensively (Yves Le Sant et al., 2001). In summary, these steps consist of background subtraction, flat field correction, image registration, wind-off and wind-on image alignment, conversion to pressure and data extraction for comparison with discrete measurements. The conversion to pressure was performed using two methods: the *in situ* and the *a priori* calibrations. The *in situ* calibration consisted of using the actual pressure tap measurements to establish the relationship between intensity and pressure during the test (Brown, 2000). The *a priori* calibration was performed independently on a PSP coupon in a controlled environment. A polynomial relationship between intensity ratio, pressure and temperature is assumed, as shown in eq. (1).

$$\frac{P}{P_{ref}} = \sum_{i=0}^{n}\sum_{j=0}^{m} a_{ij}\left(\frac{I_{ref}}{I}\right)^{i}(T)^{j} \tag{1}$$

where a_{ij} are the polynominal coefficients, n and m are the polynominal order (usually $n = m = 3$) and P_{ref} and I_{ref} are the reference pressure (1 bar) and the corresponding intensity. Depending on the PSP used, the fitting accuracies between 0.35 mbar (Unifib, NRM2) and 1.00 mbar (Unicoat, NPM2) were achieved within the calibration ranges of 0.34 bar < P < 1.3 bar and 10°C < T < 35°C.
Since model surface temperature is needed, the following *a priori* schemes have been assessed in this study.

1) The simplest assumption is that of a uniform temperature on the model. In the following, this approach is referred to as '*a priori T = RTD*' when the average of the RTD temperatures measured on the model is used.
2) Knowing (P, I) at the pressure tap locations, a local "*in situ*" temperature can be inferred from the *a priori* calibration. This tap or *in situ* temperature is likely to vary from tap to tap and its average value, T_a, can be considered as the uniform surface temperature. This approach, combining *in situ* (the tap data) and *a priori* methods, is referred to as '*a priori* $T_{in\ situ}$ or, for brevity, '*a priori* T_a'.
3) For a non-uniform model temperature assumption, an alternative approach is the iterative

computation of the local surface temperature. From an initial uniform value, (e.g. $T = T_i$ the free stream static temperature) the PSP surface pressures can be inferred (step 1) using the *a priori* calibration and local Mach numbers and recovery temperatures are then calculated assuming an isentropic flow. New surface pressures (step+1) are computed using the new local temperatures until the RMS pressure difference between two steps is small (e.g. 1 Pa). In the following, this approach is referred to as '*a priori iteration*'.

4) The local surface temperature can also be measured using an infrared (IR) camera. The corresponding result is termed the '*a priori infrared*' or '*a priori IR*' approach.

In some cases, pressure measurements from one tap have been used to remove the residual bias error from the PSP *a priori* results, thus correcting for global illumination or temperature changes and for paint photodegradation.

5. Results

5.1 Comparison of in situ Calibration and a priori Calibrations

During the first phases of the PSP test, the results obtained on the centerline station (station 1) using *in situ* and *a priori* calibrations were sometimes in agreement with the tap data. Away from the tap locations, however, the various methods gave different minimum C_p values, and thus showed different magnitudes of flow acceleration at the front windshield header (x/l = 0.367) where the main suction peak is located. Following this observation, additional pressure orifices (taps A and B in Fig. 2) were added to establish the correct values of the suction peaks on the model. The minimum C_p measured by the Tap A (x / l = 0.367) was C_p = –2.25.

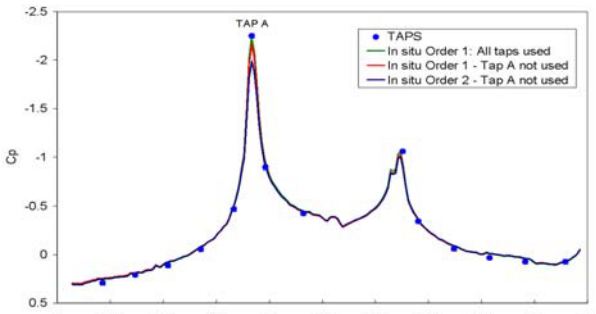

Fig. 3. PSP results obtained using *in situ* calibration on station 1. PSP obtained from phase 2, PSP Unifib, V=92 m/s. Height of symbols corresponds to ±1 mbar or ±0.02C_p. Reference is at very low speed (Pseudo-Ref at 2 m/s).

Figure 3 illustrates the effect of an additional tap on the front windshield header, Tap A at x/l = 0.367, on the *in situ* calibration on station 1. The station 1 was selected because the other stations are not exposed to such great pressure variation. For the PSP results in Fig. 3, the second additional Tap B, at x/l=0.651, was not used. The accuracy outside the main suction peak (x/l = 0.367) is not sensitive to the various *in situ* calibrations. On the other hand, the minimum C_p: –2.23 (with all taps), –2.16 (1st order, no A) and –1.99 (2nd order, no A), differs significantly depending on whether the additional tap at x/l = 0.367 is used in the calibration. When the tap on the main suction peak (Tap A) is not used, a linear *in situ* calibration is preferable to a second-order polynomial fit, to minimize the extrapolation error. In the following and for every PSP formulation, the *in situ* calibration results have been obtained using a linear fit.

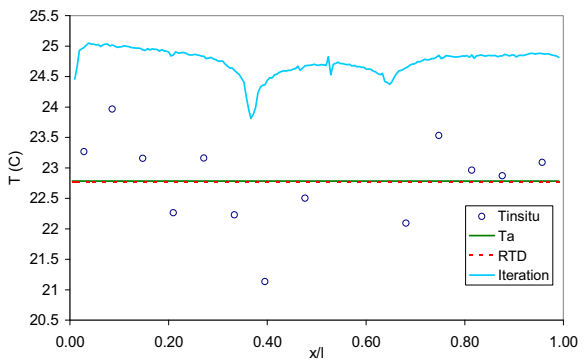

Fig. 4. Example of temperature distributions used for *a priori* data reduction methods: Phase 1: PSP Unifib, V=92 m/s, Yaw angle=0º, T_o=25.4°C. Station 1.

Unlike the *in situ* calibration, the result obtained via the *a priori* calibration is not sensitive to the number of taps or to their distribution on the model, but depends upon the choice of the wind-on and wind-off temperatures and other parameters such as light source stability or photodegradation. In the case of the Unifib paint, for instance, a simulated temperature error of 1°C on the model surface temperature had a similar influence to that induced by 0.5% photodegradation between the reference and the wind on measurements. The result of the δT=1°C error had the opposite effect if simulated on the wind-on or wind-off images and varied weakly with pressure between δC_p=0.11 and δC_p=0.13 at C_p= –2.35 and C_p= +0.5 respectively (V=92m/s, Q=51mbar, PSP Unifib).

In order to illustrate the various *a priori* calibration schemes described above, the various surface temperatures are shown in Fig. 4 for the case of Unifib at V=92 m/s (phase 1). T_{insitu} is the temperature deduced from tap pressures and intensities using the *a priori* calibration. T_a is the average of T_{insitu}. *RTD* refers to the measured surface temperature using the RTD sensors. *Iteration* is the adiabatic wall temperature iterated from PSP (after seven iterations) using r=0.895. This example is remarkable in that the average *in situ* temperature T_a is very close to the measured *RTD* temperature (within 0.02°C). The adiabatic wall temperature (*iteration*) is off from the RTD measurement by roughly 2°C, except in the suction regions, where the flow acceleration leads to a lower *iteration* temperature. The corresponding pressure coefficients obtained on the model centerline are shown in Fig. 5.

The results in Fig. 5 are taken from the first phase of the test, where Taps A and B on the suction peaks were not present. However, the tap data at the suction peaks measured in the third phase have been added to Fig. 3. The *in situ* calibration is shown with various *a priori* data reduction methods. The *a priori iteration* result has been offset using only one tap measurement, at x/l = 0.88, by ΔC_p = 0.25: the *a priori* result obtained with a higher wind-on temperature (see Fig. 4) gave a lower C_p value. After this offset correction, the *a priori iteration* showed excellent agreement with the pressure taps even at the suction peaks. The *a priori iteration* using the constant temperature assumptions (T_a and *RTD*) also showed good agreement with the pressure taps, but overestimated the suction peak slightly, suggesting that the temperature is probably lower in this region. The resulting C_p errors computed for all taps of station 1, Taps A and B excluded, are 0.037, 0.089 and 0.067 RMS, respectively, for the *in situ*, the *a priori* T_a (and *RTD*) and the shifted *a priori iteration* calibrations.

The average *in situ* temperature (T_a) and the *RTD* temperatures did not always coincide, as shown in Fig. 6, obtained from phase 3 of the test. The average *in situ* temperature T_a inferred from the tap data in

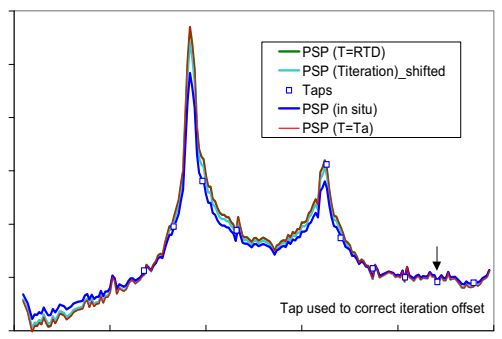

Fig. 5. C_p distributions obtained on station 1 from *a priori* and *in situ* data reduction methods (Taps A and B not used in calibration): Phase 1: PSP Unifib, V=92 m/s, Yaw angle=0°. Corresponding temperatures are shown in . Height of symbols is ±1 mbar. Reference is Pseudo-Ref (at 2 m/s).

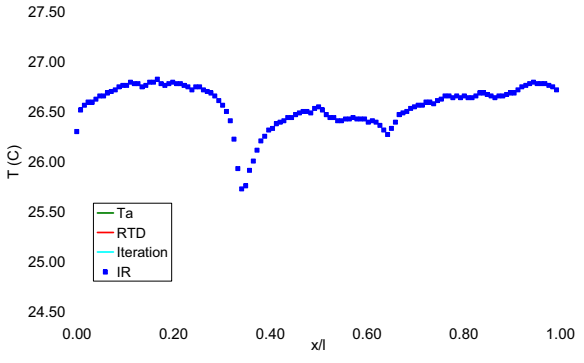

Fig. 6. Example of temperature distributions used for a priori data reduction methods: Phase 3: PSP Unifib, V=92 m/s, Yaw angle=0°, T_o=27°C. Station 1.

this example exceeds the model temperature given by the infrared (*IR*) camera or the RTD sensors because the *in situ* temperature compensates for excitation changes (estimated at 0.3% per hour) and paint photodegradation between wind-off and wind-on measurements. The *iteration* temperature was found to underestimate the measured *IR* temperature by less than 1°C. Nevertheless, it is interesting to note the qualitative agreement between the *IR* and the *iteration* temperatures because of the low thermal conductivity of the model.

The wind-on and wind-off infrared images, corresponding to the result in Fig. 6, are shown in Fig. 7. Compared to the temperature sensitive paint technique, which also requires a wind-off measurement, one obvious advantage of the infrared measurement is that it provides the wind-off model temperature distribution. In the example shown, the wind-off temperature varied by almost 1°C on the model partly because not enough time was allowed for the model to cool from the previous test at high speed (high temperatures) and partly because the ZOC module operation in the model was generating heat. In the following, a correction for the wind-off temperature distribution was performed only for the *a priori infrared* calibration.

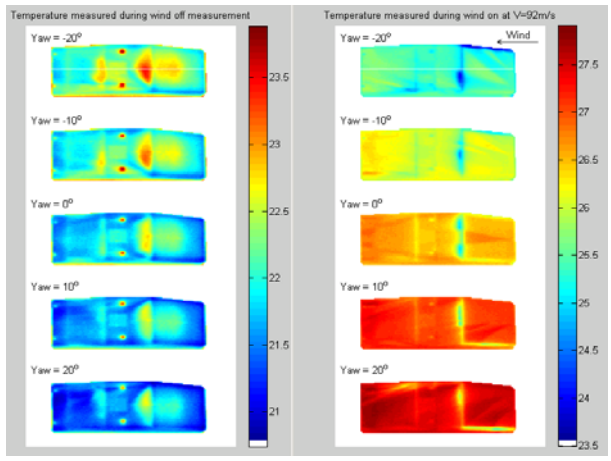

Fig. 7. Infrared measurements during wind-off and wind-on measurements. Phase 3: PSP Unifib. Station 1 highlighted in the top image. Wind-off measurement is taken before the run (Pre-Ref).

Even with this temperature correction capability, the *a priori infrared* calibration remains sensitive to global sources of errors, as discussed above (excitation change and photodegradation). This is the reason that the offset correction using one tap was implemented for all the *a priori* schemes, except for *a priori* T_a, which was already using the taps. The results are shown in Fig. 8, where the needed offset corrections were: ΔC_p = –0.10, –0.20 and –0.09, respectively, for the *a priori RTD*, *a priori iteration* and *a priori infrared* schemes. The agreement between PSP and taps on station 1 is then excellent in the case of the *a priori and the in situ* calibrations as shown in Fig. 8. It is believed that the linear *in situ* calibration performed so well, even with temperature gradients, because the small temperature variations correlated well with the pressure variations, and because of the relatively low temperature sensitivity of the PSP. The RMS C_p error at station 1 is 0.055, 0.067, 0.0845, 0.064 and 0.053 for the *in situ* calibration, the *a priori* T_a, *RTD*, and *IR* schemes, respectively.

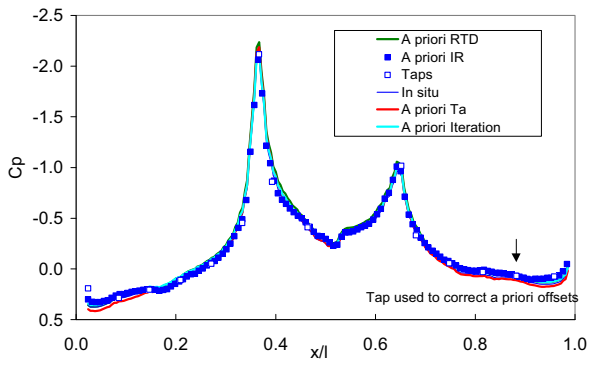

Fig. 8. C_p distributions obtained on station 1 from *a priori* and *in situ* data reduction methods (all taps used in calibration): Phase 3: PSP Unifib, V=92 m/s, Yaw angle=0°. Corresponding temperatures shown in and . Wind-off measurement taken before the run (Pre-Ref).

5.2 Summary and Discussion

The results obtained using the various data reduction methods presented above are summarized in Table 3. Errors are presented in terms of pressure (mbar) to examine the variation of absolute error with the data reduction method for all the paint formulations. The RMS error for the first test

phases (or 1 standard deviation σ) have been computed using either the 13 taps on station 1 or the 34 taps on the seven stations (see Fig. 2), to evaluate the effect of the number of stations on accuracy. For the second phase of the test, five stations on top of the model were used, except with Unifib, where one station on the model back window was excluded due to blocked ports. For the third phase of the test, a comparison with all 15 taps (Taps A and B included) on station 1 was performed. The resulting RMS errors were then averaged for all wind-on images available for each paint formulation. The PSP accuracy with respect to wind velocity is given later for the Unifib, for which more data was available.

It is interesting to note that the number of stations had a relatively small influence on the error: when the *in situ* calibration was used, the calibration using only one station provided improved accuracy. The Unifib, NRM2 and even the Unicoat (when more time for model thermal equilibrium was allowed in phase 3) provided good accuracy using linear *in situ* calibrations. Except in the case of Unicoat, the *a priori* calibrations were also satisfactory due to the offset correction compensating for light source drift, paint degradation (Unifib) and ageing (NRM2). The PTMSP formulation, NPM2, was disappointing both in terms of surface finish and accuracy. It is expected that the NPM2 sensitivity on the model was different than expected. Its sensitivity on the sample painted with the model could not be evaluated after the test due to sample ageing. Moreover, an effect of sample preparation on PTMSP stability and sensitivity has been reported in the literature (Egami et al., 2001). During most of the early phases (1 and 2), the ZOC module was operated with the heaters on to stabilize its temperature at around 30°C. This dramatically reduced the accuracy of the NPM2 and Unicoat, which were probably the most temperature sensitive formulations.

Table 3. Summary of the RMS pressure error in mbar from the different data reduction methods averaged over all the wind-on images available processed using various wind-off images: before run (pre-ref), after run (post-ref) and at 2 m/s (pseudo-ref) when available.

PHASE	PSP	IN SITU Error (mbar)	A PRIORI Error (mbar)				# Stations	# Taps per image	# Wind on images	# Wind off / Wind on combinations
			T=Ta	T=RTD	Iteration	T=IR				
1	UNIFIB	2.62	5.46	6.65	5.72	-	1	13	13	17
		4.48	5.84	6.13	5.90	-	7	34	13	17
1	UNICOAT	4.36	42.18	62.82	37.18	-	1	13	8	13
		8.54	34.04	55.74	31.73	-	7	34	8	13
2	NPM2	4.48	38.92	14.18	14.62	-	1	13	8	10
		3.96	34.76	11.67	12.03	-	4	27	8	10
2	NRM2	1.84	5.97	6.95	6.40	-	1	13	6	9
		2.08	5.76	6.31	5.88	-	4	27	6	9
2	UNIFIB	3.42	6.00	7.02	5.89	-	1	13	27	57
		4.50	6.19	6.96	6.07	-	4	24	27	57
3	UNICOAT	3.73	12.34	15.45	10.77	10.95	1	15	17	49
3	UNIFIB	3.38	5.90	6.68	6.00	5.84	1	15	37	57

A large number of wind-off images were acquired before (Pre-Ref) or after (Post-Ref) each run and acquisitions at a very low wind speed (Pseudo-Ref) were also used as reference. Only the most reasonable combinations of wind-off/wind-on ratios were evaluated in this study. Before correction of the *a priori* results, it was noticed that the choice of the wind-off image had some influence on the accuracy. However, this influence was considerably reduced with the *a priori* offset corrections using the same tap on station 1 (located at $x/l = 0.88$). These *a priori* offset corrections were not effective for the Unicoat (phase 3) which is too sensitive to temperature and would require a different scheme to correct for small temperature variations (Bencic, 1999).

Table 4 presents the details of the PSP Unifib performance as a function of wind speed and

for various types of reference images. The Pre-Ref and Post-Ref references are true wind-off (zero speed) images acquired before and after the corresponding runs respectively, whereas Pseudo-Ref refers to images acquired at very low speed (V=2 m/s) generally after the high speed runs (V=92 m/s). The infrared measurements in phase 3 revealed that the low air speed was sufficient to stabilize the model temperature. Although no infrared measurement was available during the first phase of the test, it seems that the low-speed airflow was also very effective in reducing the influence of the ZOC module heating in the model. The errors obtained at V=92 m/s and V=41 m/s were minimal in the case of the Pseudo-Ref. However, other true wind off images provided good results when the wind-off measurement was made close in time with the wind-on measurement (e.g. at 62 m/s or 41 m/s). The minimum errors obtained for each speed have been extracted from Table 4 without consideration of the nature of the reference and plotted as a function of the wind speed V and the dynamic pressure Q in Fig. 9 and Fig. 10. The pressure errors increase almost linearly with respect to the wind speed and the *in situ* error is consistently lower than the others by roughly 2 mbar. On the other hand, the influence of the decreasing dynamic pressure is predominant in the C_p error at speeds below 40m/s; at high dynamic pressure, the Cp error reaches a minimum of 0.05 at 75 m/s.

Table 4. RMS pressure error in mbar for the Unifib obtained from all three phases of the test.

V (m/s)	Q (mbar)	IN SITU Error (mbar)	A PRIORI Error (mbar)				Type of Reference	# Wind on images
			T=Ta	T=RTD	Iteration	T=IR		
92	51.1	5.00	8.06	10.80	9.14	6.34	Pre-Ref	32
		5.38	7.87	9.00	7.80	6.69	Post-Ref	11
		2.97	5.46	6.01	6.01		Pseudo-Ref	30
77	35.8	1.85	4.15	4.53	3.49	-	Pre-Ref	1
62	23.2	2.23	3.26	5.23	4.46	-	Pre-Ref	3
		1.53	4.36	4.38	3.81	-	Post-Ref	1
		4.39	4.65	5.05	4.76	-	Pseudo-Ref	3
41	10.1	1.99	6.52	7.40	6.28	6.97	Pre-Ref	6
		2.55	7.60	8.37	7.86	11.23	Post-Ref	12
		1.01	3.48	4.07	3.63		Pseudo-Ref	4
27	4.3	0.84	2.24	2.52	2.30	1.56	Post-Ref	5
11	0.73	0.30	2.53	2.64	2.52	2.23	Post-Ref	5

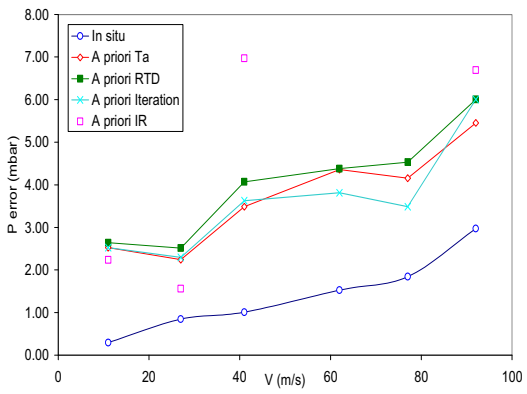

Fig. 9. RMS pressure error for PSP Unifib averaged over the three phases of the test.

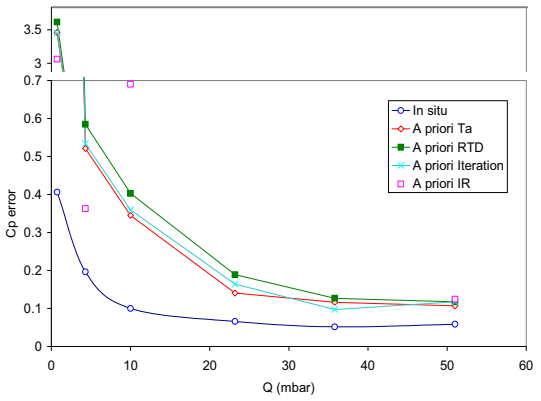

Fig. 10. C_p errors for PSP Unifib averaged over the three phases of the test.

5.3 PSP as a Visualization Tool

The images presented in this section were obtained using *in situ* calibration from the centreline station. PSP not only provides quantitative pressure measurement, it can complement usual visualization techniques. During this test, surface flow visualization was used to show the surface flow features. The oil drops were applied directly on top of the PSP Unicoat and images of the surface flow development were recorded using the PSP camera. Because the oil streaks reduced the PSP intensity, the evolution of the intensity level in these images revealed the path followed by the oil streaks. The resulting negative oil flow images are presented in Fig. 11. The infrared images, showing the surface temperature changes due to turbulent wedges or to local flow acceleration, are also presented in Fig. 11 along with the PSP images at the same conditions.

Since the oil flow images were taken with the same CCD camera as that used for PSP, they were mapped onto the grid of the model and the background was removed. The oil flow images were also blended with the PSP images shown in Fig. 11, and the result is presented in Fig. 12. The regions of high and low pressure are still represented by hot and cold colours respectively, but the quantitative aspect of the PSP has been lost in the process. Nevertheless, the understanding of the pressure field was enhanced with the oil visualisation of vortices and of separated flow regions (e.g. on the rear window at 0° angle) on the model.

During the last phase of the test, the speed was reduced to 11 m/s and 32 images were averaged to reduce the noise and provide a useful view of the pressure field as seen in Fig. 13. The extended low-pressure region on the roof is clearly visible at this speed.

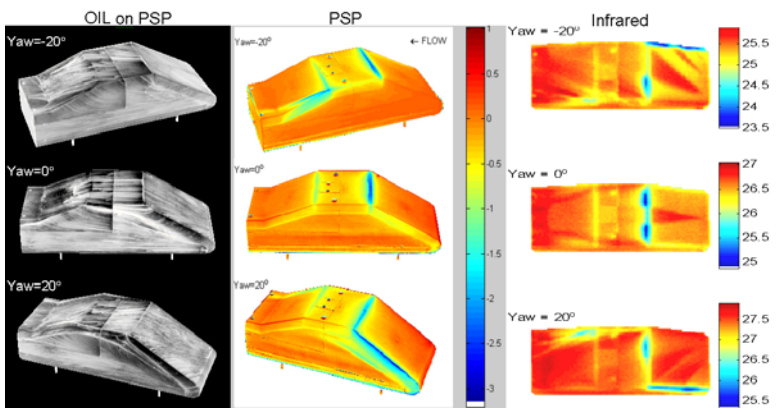

Fig. 11. Oil flow visualization on PSP (inverted image), PSP image (C_p results from PSP Unifib) and infrared measurements (temperature in °C) at V=92 m/s. Phase 3. PSP: 32 images per angle. Post-Ref used.

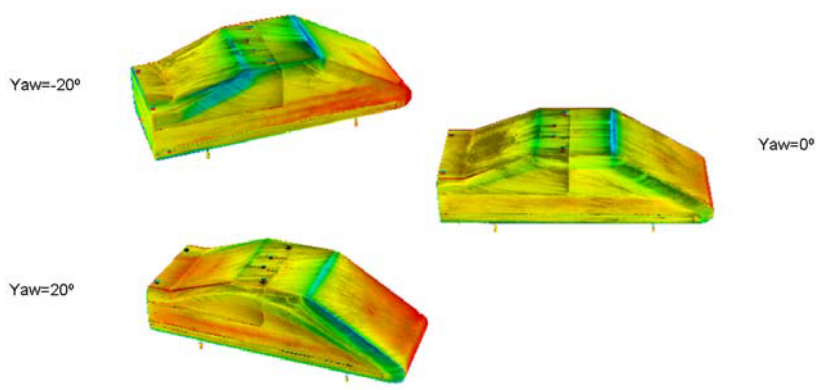

Fig. 12. Blending of oil flow visualization and PSP results.

The noise levels in the PSP images can be reduced if a sufficient number of images are averaged to reduce the photon shot noise. In general, the number of images used varied from 8 to 64, depending on the run speed and only the resulting average was saved. However, in several instances, it was decided to save all 64 images and to perform averages of different numbers of the images, 4, 8, 16, … up to 64, to examine the effect on the resulting intensity ratio. The results are shown in Fig. 14 for the PSP Unicoat (Phase 3). It was found that the intensity ratio standard deviation $\sigma(I_{ref}/I)$, extracted from a small region of uniform I_{ref}/I, followed roughly the inverse of the square root of the number of images: 1.65×10^{-3} with 4 images, 0.57×10^{-3} with 32 images and 0.4×10^{-3} with 64 images. No significant improvement is visible on Fig. 14 beyond 32 images at 27 m/s. A temperature gradient induced by the thermal inertia of the aluminium plates (on the model top and side) is visible for the first images and then attenuates towards the end of the run. After this run, several minutes were allowed after each speed change in order to permit the model to reach thermal equilibrium with the flow. The infrared camera, showing the temperature in real time, was useful in determining that temperature equilibrium had been achieved.

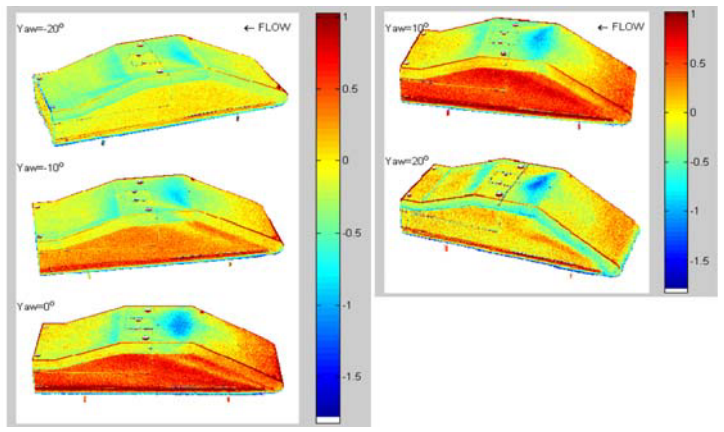

Fig. 13. C_p images. PSP Unifib at 11 m/s. Phase 3: 32 images averaged per angle. Post-Ref used.

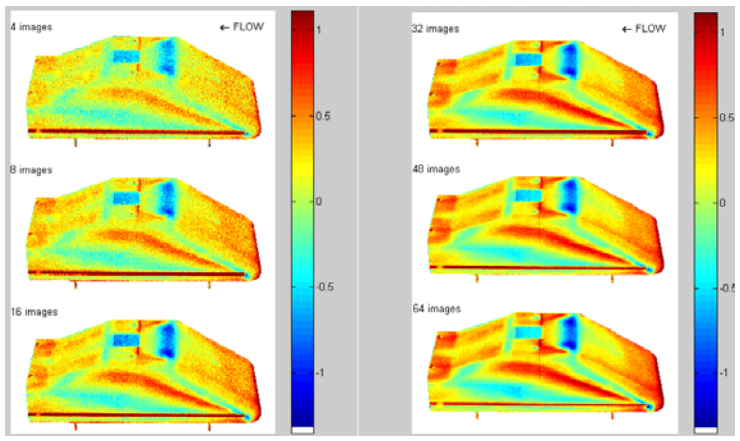

Fig. 14. C_p images Yaw angle=0º. Effect of image averaging on noise *V*=27 m/s for PSP Unicoat.

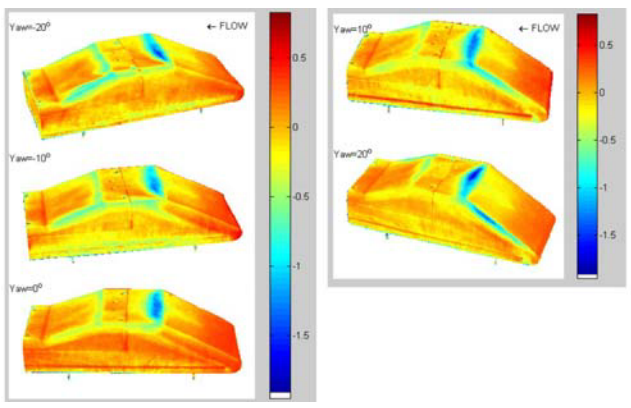

Fig. 15. C_p images obtained for PSP Unicoat at 27 m/s. 64 images per angle. Phase 3. Post-Ref used.

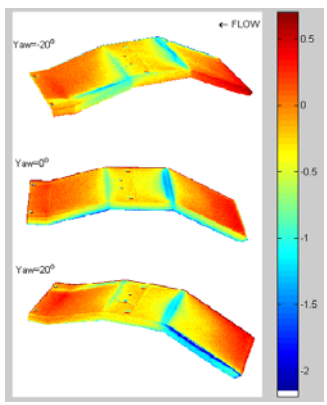

Fig. 16. C_p images obtained for PSP Unifib at 41 m/s. 64 images averaged per angle. Phase 3.

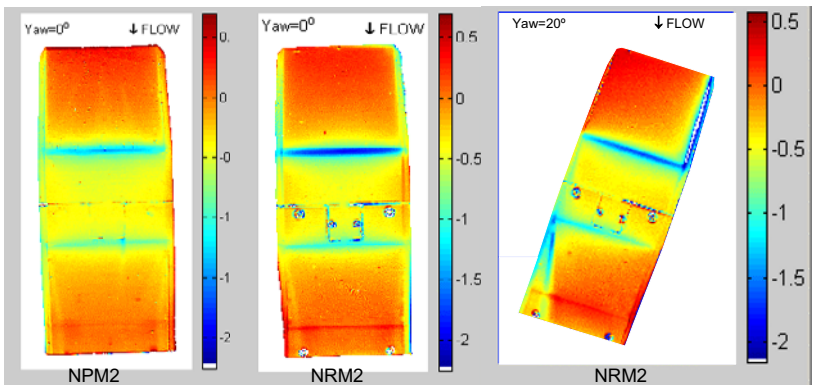

Fig. 17. C_p images obtained for pyrene-based PSP. Phase 2. *V*=92 m/s. 16 images averaged. Post-Ref used.

When the model temperature was allowed to stabilize, the PSP Unicoat revealed the pressure field at 27 m/s (Fig. 14), without showing the presence of the aluminium components visible on the side and the top of the model in Fig. 14. The PSP accuracy of Fig. 15 is 0.19 in C_p or 0.84 mbar. The size of the low-pressure region on the model roof/windshield junction is reduced at 0° yaw compared to that observed at 11 m/s. In the second phase of the test, the PSP Unifib was used with an ultraviolet light. The results obtained at *V*=41 m/s for three yaw angles, with an accuracy of 0.047 in C_p or 0.48 mbar, are shown in Fig. 16. The extent of the low-pressure region on the roof is further reduced below V=27 m/s, with sharp vortices being visible on the model back window. The results obtained with the pyrene formulations, are shown in Fig. 17. The quadratic error was 0.071 in C_p for the NPM2 and 0.017 to 0.021 in C_p for the NRM2 images shown. On these images, the effect of the two vortices on the back window is barely visible at 0º-yaw angle.

6. Conclusion

A PSP evaluation was conducted using a simplified car model at the IAR 2 m x 3 m continuous atmospheric wind tunnel. Image averaging permitted accurate data to speed as low as 27 m/s and qualitative measurements at 11 m/s. Several paint formulations, including in-house and commercial types have been used. In particular, a formulation combining PTMSP and pyrene was applied for the first time in the low-speed regime.

The early PSP results found two sharp suction peaks that were missed by the pressure taps. The high resolution PSP results were used to position two additional taps at those locations. This example clearly shows one benefit of the PSP technique. The linear *in situ* calibration, sufficient for all paint formulations, provided a better accuracy than the *a priori* methods. However, the tap distribution was critical for the precision of the *in situ* results.

Pressure tap data were used in combination with *a priori* calibrations to determine the model surface temperature. These temperatures did not always agree with infrared or RTD measurements, probably due to the uniform sources of error such as excitation changes and photodegradation.

The *a priori* calibrations provided good agreement with pressure taps for Unifib and NRM2 formulations when only a single tap was used to correct for these bias error sources. The assumption of a uniform temperature on the model over the range of speeds tested was then a good approximation everywhere, except in localized accelerated flow regions. This suggests that for a non-conductive model, surface temperature iteration or measurement is required to capture the peak suction pressures accurately.

Acknowledgements

This work has been conducted at the Institute for Aerospace Research as part of a research program aimed at the implementation of the PSP technique in IAR low-speed facilities. The authors acknowledge Yves Le Sant, for his help with the AFIX2 software, and Marie Claire Mérienne for many helpful suggestions about the pyrene-based formulations. The authors are grateful to the reviewers for their constructive comments.

References

Asai, K., Amao, Y., Iigima, Y., Okura, I. and Nishida, H., Novel Pressure-Sensitive Paint for Cryogenic and Unsteady Wind Tunnel Testing, J. of Thermophysics and Heat Transfer, 16-1 (2002).

Bencic, T. J., Pressure-Sensitive Paint Measurements on Surfaces with Non-Uniform Temperature, Proceedings of the International Symposium on Instrumentation in the Aerospace Industry, (1999).

Benne, M. E., Kammeyer, M. E., Donovan, J. F., Rueger, M. L., Harris, J. N., Morgenroth, D. M. and Green, E., General Strategy for the Development of an Improved Pressure-Sensitive Paint Formulation, AIAA Paper 2002-2906, AIAA conference, St Louis, (2002).

Bell, J. H., Schairer, E. T., Hand, L. A. and Mehta, R. D., Surface Pressure Measurements Using Luminescent Coatings, Ann. Rev. Fluid Mech., 33 (2001).

Brown, O., Low Speed Pressure Measurements Using Luminescent Coatings, PhD Thesis, Stanford University, USA, (2000).

Crites, R. C., Measurement Techniques: Pressure Sensitive Paint Technique, VKI Lecture Series 1993-05.

Egami, K., Iigima, Y. and Asai, K., Optimization of Polymer-Based PSP for Cryogenic Wind Tunnels, ICIASF (2001).

Khalil, G., Gouterman, M., Ching, S., Costin, C., Coyle, L., Gouin, S., Green, E., Sadilek, M., Wan, R., Yearyean, J. and Zelelow, B., Synthesis and Spectroscopic Characterization of Ni, Zn, Pd, Pt Tetra(pentafluorophenyl) Porpholactone with Comparisons to Mg, Zn, Y, Pd, Pt Metal Complexes of Tetra(pentafluorophenyl) Porphine, Journal of Porphyrins and Phtalocyanines, 6 (2002).

Kulesh, V. P., Morozov, A. N., Mosharov, V. E. and Radchenko, V. N., Application of a Prism Image Splitter for Pressure Distribution Measurement using Two-Color Luminescent Sensors, Instruments and Experimental Techniques, 44-1 (2001).

Liu, T., Campbell, B. T., Burns, S. P. and Sullivan, J. P., Temperature and Pressure Sensitive Paints in Aerodynamics, Applied Mechanics Reviews, 50-4 (1992).

Le Sant Y., Bouvier, F. and Mérienne, M. C., Mesures de la Pression Pariétale à l'Aide de Peintures Sensibles à la Pression, 9th FluVisu Conference, Rouen, (2001).

Mérienne, M. C., Pesonnal communication, (2001).

Mérienne, M. C. and Soumagne-Schweyckart, I., New pyrene-based formulation for PSP applications, RT 217/05458 DAFE, (2002).

Mitsuo, K., Hayasaka, M., Kameda, M. and Asai, K., Temperature Correction of PSP Measurement using Dual Luminophore Coating, 10th Intern. Symp. on Flow Visualization., Kyoto, (2002).

Author Profile

Youssef Mébarki: He has obtained a Ph.D. in the field of Mechanical Engineering from the University of Lille (France) in 1998. He is presently a Research Officer in the Aerodynamics Laboratory of the National Research Council (NRC) of Canada. His current research activities include development and implementation of Pressure Sensitive Paint technique in NRC low speed and high speed facilities.

Kevin Cooper: He is a Principal Research Officer in the Aerodynamics Laboratory of the National Research Council of Canada. He has 35 years experience in experimental aerodynamics. His specialities have been the aerodynamics of bluff bodies, focussing primarily on surface vehicles and civil engineering structures. He has been the manager of the 9m wind tunnel and the other low-speed wind tunnels of the NRC. He has currently returned to full-time research.

Todd Reichert: He is completing his second year of Aerospace Engineering and Cinema Studies degree at the University of Toronto. He has worked for Nortel Networks and for the Eye Institute at the Ottawa General Hospital. His collective interest in photography and engineering led him to work on Pressure Sensitive Paint techniques in the Aerodynamics Laboratory of the National Research Council during the summers of 2001 and 2002.